ARTICLE **Open Access**

Whispering-gallery-mode full-color laser textiles and their anticounterfeiting applications

Jun Ruan[1], Dan Guo [1], Ben Niu[1], Kun Ge[1] and Tianrui Zhai [1]

Abstract
Light-emitting fabric can facilitate the innovation of wearable display applications. Electronic and luminescent textiles capable of communicating, sensing, and supplying energy have been achieved. However, a facile strategy for fabricating large-area flexible lasing textiles has not yet been reported. In this work, we propose a gravity-assisted rotatory drawing method for fabricating flexible lasing microfibers, which can be woven into multicolor lasing textiles. By regulating the doped dyes and solution viscosity, we achieve the mass manufacturing of lasing microfibers with different emission colors and modes and further weave them into full-color textiles with a wide color gamut, approximately 79.1% larger than that of standard RGB space. For application, we print nanoparticle patterns on the lasing textile and encode it with programmable lasing signal distribution, which can supply an anticounterfeiting label for efficient authentication. This work unifies the fabrication and application of lasing textiles, and we expect that this will provide a new platform for flexible lasing devices.

Introduction

Integrating light into textiles facilitates numerous new perspectives for wearable technology, personal safety, fashion, and medical therapy[1−3]. In recent decades, the development of light-emitting fabric has offered exciting opportunities for smart textiles due to their deformable, porous, and robust characteristics that are important for bridging human–machine interactions[4,5]. With their good chromaticity of emissions, high contrast ratio, and vivid colors, laser displays are undergoing rapid development in flat-panel displays[6], as well as evolution in flexible devices[7]. In recent years, ever-increasing efforts have been made regarding the preparation and optoelectronic applications of microlaser arrays, which significantly expands the capabilities of the microlasers[8]. However, large-area lasing textiles have not yet been reported.

As the basic component, micro/nanolasers with small sizes, low thresholds, and capacities of on-chip integration are widely studied by researchers[9−12]. The whispering-gallery-mode (WGM) microcavity, which traps light inside the cavity via internal total reflection to enhance light-matter interaction, has shown a high-quality factor and small mode volume[13,14]. Moreover, the fabrication approach shows good compatibility for many processing strategies, such as microfabrication[15], solution-based self-assembly[16], inkjet printing[17,18], and electrospinning[19,20], which is beneficial for the effective integration of functional devices. To date, WGM laser integrated devices have been used in widespread applications in full-color laser imaging[21], biological or chemical sensing[22−25], on-chip optical communication[26,27], encryption[28,29], etc.

A wide variety of materials, including glass[30], semiconductors[31], and polymers[32,33], have been used to make WGM resonators. Among these, polymer-based WGM cavities have attracted extensive attention due to their mechanical flexibility and good biocompatibility. In particular, polymer microfibers cannot only supply resonant cavities[34] but also serve as typical flexible materials applied in wearables[35]. Therefore, polymer materials may be potential candidates for manufacturing lasing textiles, and the problems of the mass production of flexible

Correspondence: Dan Guo (dguo@bjut.edu.cn) or
Tianrui Zhai (trzhai@bjut.edu.cn)
[1]College of Physics and Optoelectronics, Faculty of Science, Beijing University of Technology, Beijing 100224, China

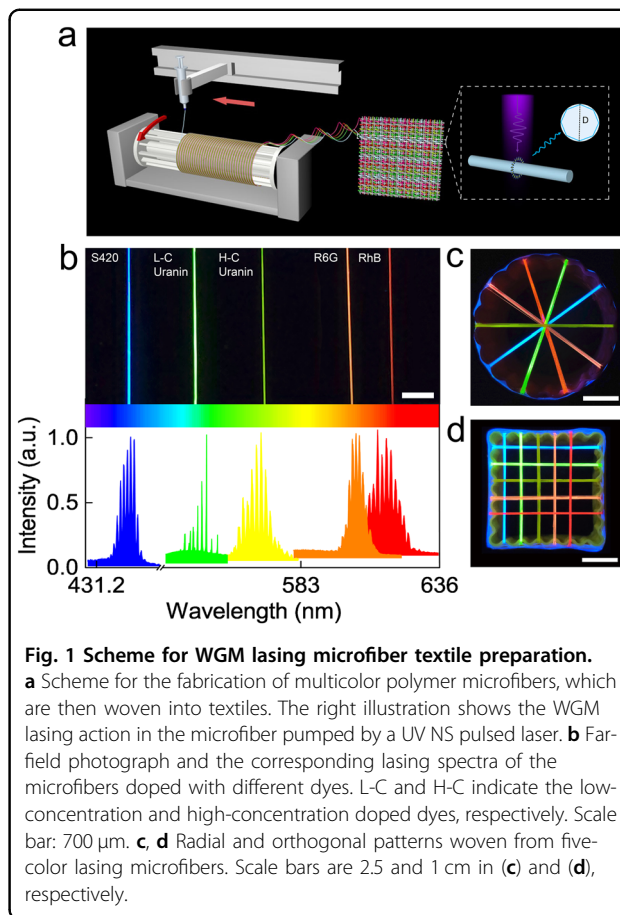polymer microfibers and weaving them into multicolor lasing textiles must be addressed.

In this work, a gravity-assisted rotary drawing method is proposed to fabricate mass-produced flexible microfibers, which can be woven into multicolor lasing textiles. By regulating the doped dyes and the solution viscosity, we achieve microfibers of different lasing emission colors and modes and weave them into full-color lasing textiles. Furthermore, we print a nanoparticle (NP) pattern on a lasing textile to encode it with programmable lasing signal distribution for anticounterfeiting applications.

Results and discussion

Fabrication of microfiber textiles

Four typical laser dyes, disodium 4,4'-bis(2-sulfonatostyryl) biphenyl (S420), fluorescein disodium salt (Uranin), rhodamine 6G (R6G), and rhodamine B (RhB), are employed as gain materials, with photoluminescence (PL) emission in blue, green, orange and red wavebands, respectively (Supplementary Fig. S1). A high-concentration uranin-doped polymer is used to supply the yellow emission through a reabsorption process, in which emitted light is absorbed by neighboring molecules and re-emitted at lower energy wavelengths[36]. The solution for microfiber fabrication is prepared by mixing polyvinyl alcohol (PVA, Mw: 198,000 g mol^{-1}), sodium dodecyl sulfate (SDS), and gain materials. The optimized concentration of PVA is set as 176 mg mL^{-1}. The addition of SDS is vital for the solution viscosity and microfiber formation. SDS can decrease the surface tension and increase the solution viscosity, which is significant for uniform microfiber formation with a controlled diameter.

The scheme of the polymer microfiber fabrication is shown in Fig. 1a. A rotary drum is employed as the microfiber collector, which can be rotated and precisely controlled by a motor. The solution in a syringe is gradually squeezed out with a slow flow rate by a peristaltic pump, and the formed microfibers are collected on the rotary drum. In contrast to electrospinning driven by a high electrostatic field, which is usually employed for thin fibers, we take advantage of gravity to assist with fiber formation. When the viscous liquid falls from a syringe nozzle, it remains attached to the source by an elongating liquid filament due to its viscosity[37]. The formed liquid filament is gradually collected by the rotary drum in succession. By optimizing the squeezing flux and rotating speed (see Materials and methods and Supplementary Video S1), the uniform viscoelastic liquid filaments are formed between the drum fins. Moreover, the syringe is mobile, which is controlled by the motorized positioning stages. Then, evenly arranged microfibers are obtained, and uniform films covering tens of centimeters can be obtained when the syringe mobility is carefully regulated. Finally, free-standing microfibers are formed after the

Fig. 1 Scheme for WGM lasing microfiber textile preparation. a Scheme for the fabrication of multicolor polymer microfibers, which are then woven into textiles. The right illustration shows the WGM lasing action in the microfiber pumped by a UV NS pulsed laser. **b** Far-field photograph and the corresponding lasing spectra of the microfibers doped with different dyes. L-C and H-C indicate the low-concentration and high-concentration doped dyes, respectively. Scale bar: 700 μm. **c, d** Radial and orthogonal patterns woven from five-color lasing microfibers. Scale bars are 2.5 and 1 cm in (**c**) and (**d**), respectively.

evaporation of the solvent (Supplementary Video S2) and can be readily detached from the drum. Owing to this method, large-area flexible lasing textiles could be obtained (Supplementary Fig. S2 and Supplementary Video S3).

Benefiting from the inter- and intramolecular van der Waals interactions in the system, the microfiber is flexible and can be woven into a multicolor film. The polymer microfibers have a cylindrical shape with a smooth outer surface (Supplementary Fig. S3), which is vital for efficient optical confinement. We are able to fabricate multicolor microfibers by doping different dyes (Fig. 1b) and obtain broad wavelength-tunable WGM lasing. Different color lasing emissions are observed from the microfiber by optical pumping from a nanosecond laser at a wavelength of 343 nm under ambient conditions (Supplementary Fig. S4). These multicolor microfibers can be readily arranged and woven into textiles (Fig. 1c, d), showing uniform bright patterns. The colors of microfibers can cover the entire visible waveband and have the potential to be used in the field of laser display.

During microfiber formation, the diameter of microfibers can be regulated by several factors, such as the drum rotating speed, squeezing flux of solutions, distance

between the syringe tip and the drum collector (Supplementary Fig. S5), and the solution itself. Among them, the viscosity of the solution is critical to microfiber formation with controllable diameters. The concentration of SDS is important for the viscosity of the solution because of the molecular interactions[38]. Under low viscosity without SDS addition, the capillary retraction of a Newtonian semi-infinite liquid filament[39] results in a microfiber that is too thin to support the internal light oscillation (Supplementary Video S4). We investigate the dependence of the SDS concentration (surpassing the critical micelle concentration) on the viscosity of the bulk solution and the diameter of the S420-doped PVA microfiber. It is found that the microfiber diameters increase with the solution viscosity and the concentration of SDS. By increasing the concentration of SDS from 10 to 50 mg mL^{-1}, the solution viscosity increases from approximately 25–175 Pa·s at 30 °C, and microfibers with gradually enlarged diameters from 4.8 to 65.3 μm can be obtained (Fig. 2a and Supplementary Fig. S6).

Lasing properties of blue-, green-, and red-color microfibers

We investigate the mode spacing of microfibers with different diameters. The value of the free spectra range (FSR) decreases with the diameter of the lasing microfibers (Fig. 2b and Supplementary Fig. S7). For a WGM cavity, the FSR can be estimated as $\lambda^2/\pi n_{cav} D$, where λ is the resonant wavelength and n_{cav} and D are the refractive index and diameter of the microfiber, respectively. The experimental data are fitted with a linear slope (πn_{cav}) of approximately 5.00 (Fig. 2c), showing that the FSR is inversely proportional to the microfiber diameter (D), verifying the WGM-type cavity resonances. The n_{cav} is calculated to be 1.59, which is in good agreement with the obtained refractive index of the mixed PVA-SDS-dye film of 1.55 measured by an ellipsometer. Supplementary Fig. S8 shows the lasing emissions of the transverse electric and transverse magnetic modes, as well as the calculated mode number (Supplementary Notes).

Based on this, we investigate the lasing properties of microfibers doped with S420, Uranin, and RhB. The corresponding PL spectra evolution with increasing pumping fluence is shown in Fig. 2d–f. At low pump fluence, the PL spectra are dominated by broad spontaneous emission. When the pump fluence exceeds a threshold, the emission spectrum develops into a set of sharp peaks, indicating stimulated emission. The plot of PL intensity and full-width at half-maximum (FWHM) versus pump fluence exhibits a clear knee-behavior characteristic, with thresholds of approximately 11.5, 10.5, and 28.1 μJ cm^{-2} for S420-, Uranin-, and RhB-doped microfibers, respectively (Fig. 2g–i), further confirming the lasing action of the microfibers. These results show that our microfibers demonstrate good lasing properties (Supplementary Tables S1 and
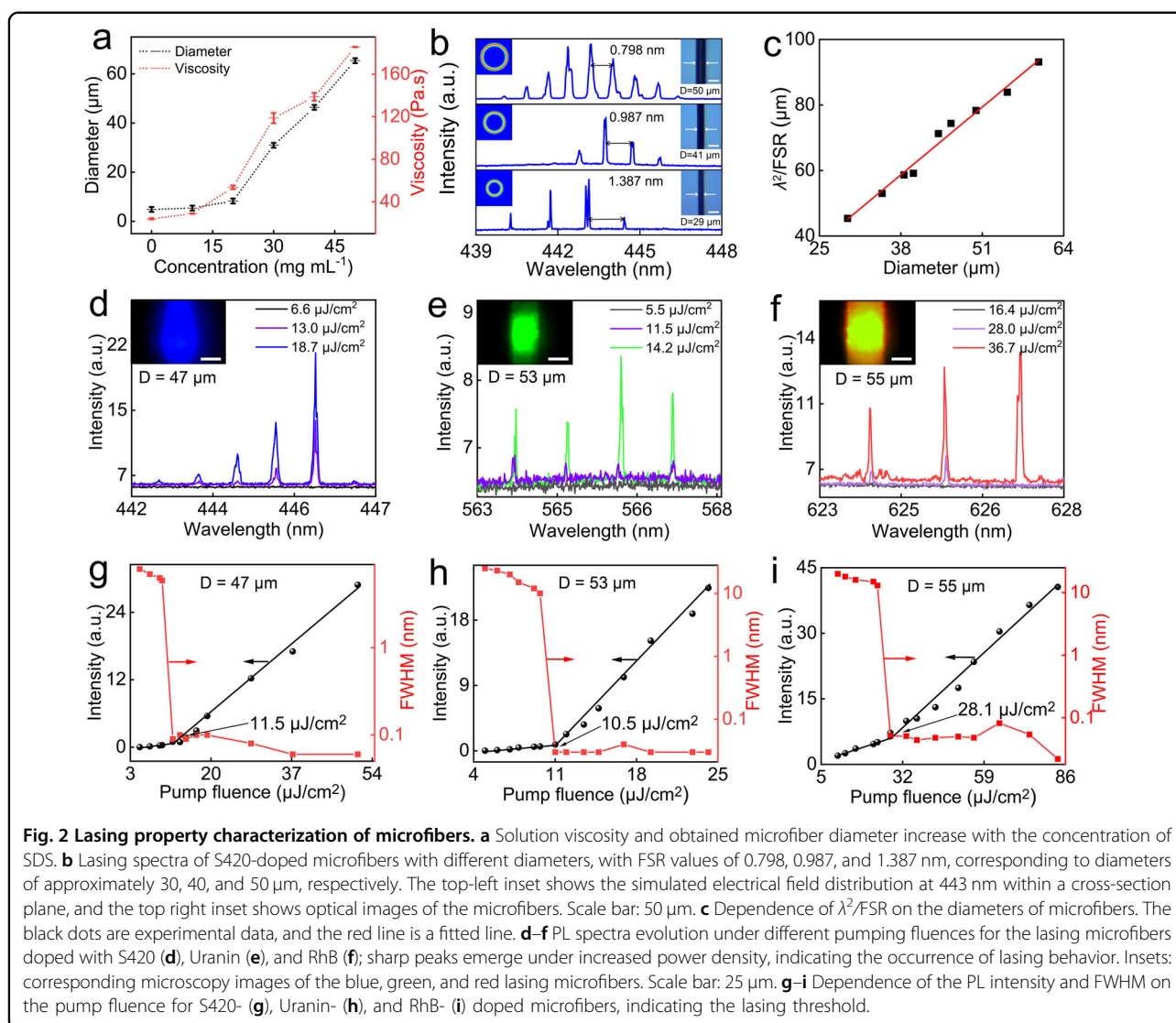
S2). The FWHM of the sharp lasing peaks can be as small as 0.03 nm according to Lorentz function fitting (Supplementary Fig. S9). According to $Q \approx \lambda_0/\Delta\lambda$, where λ_0 and $\Delta\lambda$ are the center wavelength and FWHM of the peak profile, the quality factor Q is calculated to be approximately 18,000. Note that the threshold of the RhB-doped lasing microfiber is higher than that of the other two dyes. This result can be attributed to the smaller absorption cross-section for RhB compared to that of the other two dyes in the ultraviolet (UV) waveband (Supplementary Fig. S1).

Weaving the microfibers into patterns for full-color display

According to Grassmann's law[40,41], all colors inside the triangle defined can be produced by mixing the three primary colors (blue, green, and red) in appropriate proportions. Here, we weave the RGB lasing microfibers into a triangle pattern to serve as a tunable lasing source, and seven typical lasing spectra are obtained by selectively regulating the pumping position and spot size (Fig. 3a). Thus, a wide color gamut can be achieved by controlled pumping simply through programming a spatial light modulator. Figure 3b shows the calculated chromaticity based on the International Commission on Illumination (CIE) 1931 color diagram. The chromaticity coordinate of the mixed white (R+G+B) lasing is very close to the coordinate of white light. In addition, the drawn triangular region according to the other six chromaticity coordinates indicates the color gamut that can be realized by mixing three primary colors in appropriate proportions. The color gamut in this work covers approximately 79.1% more perceptible colors than the standard RGB color space (Supplementary Table S3) and thus could support vivid colors for full-color flexible displays. Moreover, we can control the number of flexible microfibers to be woven into different patterns (Fig. 3c), indicating the potential to tune the color temperature[42].

Printing on lasing textiles for anticounterfeiting

The lasing microfibers are flexible and stable (Fig. 4a and Supplementary Fig. S10) and can be readily woven into textiles with good tensile strengths (Supplementary Fig. S11). Considering that PVA is a water-soluble polymer (Supplementary Video S5), we treated the formed PVA microfiber with glutaraldehyde vapor to obtain waterproof microfibers (see Materials and methods). The crosslinking reaction proceeds with the formation of acetal bridges between the hydroxyl groups in PVA and the difunctional aldehyde groups in glutaraldehyde[43]. This posttreatment makes the microfibers waterproof (Fig. 4b and Supplementary Video S6) and has almost no impact on the lasing properties of the microfibers (Supplementary Fig. S12). In addition, the morphologies and lasing properties of the posttreated microfibers are perfectly retained even after being soaked in water for 24 h (Supplementary Figs. S13–S15). Moreover, the lasing properties of the bent

Fig. 2 Lasing property characterization of microfibers. a Solution viscosity and obtained microfiber diameter increase with the concentration of SDS. **b** Lasing spectra of S420-doped microfibers with different diameters, with FSR values of 0.798, 0.987, and 1.387 nm, corresponding to diameters of approximately 30, 40, and 50 μm, respectively. The top-left inset shows the simulated electrical field distribution at 443 nm within a cross-section plane, and the top right inset shows optical images of the microfibers. Scale bar: 50 μm. **c** Dependence of λ^2/FSR on the diameters of microfibers. The black dots are experimental data, and the red line is a fitted line. **d–f** PL spectra evolution under different pumping fluences for the lasing microfibers doped with S420 (**d**), Uranin (**e**), and RhB (**f**); sharp peaks emerge under increased power density, indicating the occurrence of lasing behavior. Insets: corresponding microscopy images of the blue, green, and red lasing microfibers. Scale bar: 25 μm. **g–i** Dependence of the PL intensity and FWHM on the pump fluence for S420- (**g**), Uranin- (**h**), and RhB- (**i**) doped microfibers, indicating the lasing threshold.

microfibers can be generally retained with a slightly higher threshold than the straight microfibers (Supplementary Fig. S16). Therefore, waterproof and bendable microfibers with stable lasing properties are achieved, showing promise for applications in large-area flexible lasing displays and wearable devices.

Based on this, a lasing textile with a "BJUT" pattern is made by weaving the lasing microfibers on a fabric mesh (Fig. 4c), which is flexible and bendable. Furthermore, we encrypt the lasing textile by inkjet printing TiO_2 NP patterns onto it (Fig. 4di). With a high refractive index, TiO_2 NPs with a diameter of 100 nm can serve as the scattering loss at the resonant microcavity surface, resulting in an optical leakage channel for interfering with the light oscillation and consequently a failing lasing property. In addition, TiO_2 NPs can absorb some UV light to some degree, supplying another loss factor. Therefore, we prepared the ink by dispensing TiO_2 NPs in ethanol, in which

the polymer matrix cannot be dissolved. After printing a few layers of TiO_2 NPs on the S420-doped lasing textile, we compare it with the unprinted textile. On the one hand, no difference can be distinguished under natural or UV light (Fig. 4dii). On the other hand, under the pumping fluence above the threshold, the area without NPs still retains the lasing property, while only fluorescence is left on the NP distribution area (Fig. 4e), indicating that the lasing property is damaged by scattering loss. Therefore, we can divide the surface area of textile into $m \times n$ cells and encode a cell with a lasing signal of "1" and a cell with a fluorescence signal of "0". With this binary coding, we can write $2^{m \times n}$ information to encrypt a textile. With this lasing textile, we can achieve information storage even using a commercial printer, which can be easily programmed by a cellphone. For example, one can easily use their cellphone to generate a unique QR code and control the printer to encrypt their clothes with an anticounterfeiting label.
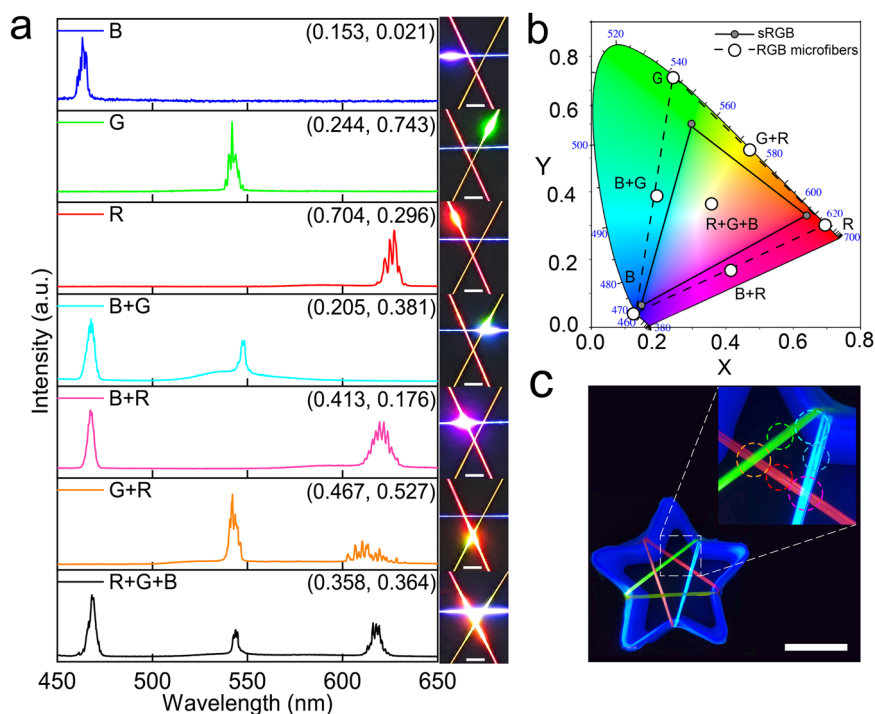
Fig. 3 Full-color display of the lasing pattern formed by woven microfibers. a Multicolor tunable lasing spectrum. The measured and corresponding PL images are obtained by regulating the pumping spots on the woven triangle pattern. From top to bottom: the blue (B), green (G), red (R), cyan (B+G), magenta (B+R), yellow (G+R), and white (B+G+R) lasing spectra. The top right inset shows the chromaticity coordinates calculated from the individual spectra. Scale bar: 1 mm. **b** CIE chromaticity diagram of the lasing emissions from the spectra in **a**, marked by seven white circles. The solid and dashed lines indicate the range of standard RGB space and the achievable color gamut of our prepared lasing textiles, respectively. **c** Woven pentangle pattern with bunches of lasing microfibers, in which both the number of microfibers and pumping position (marked by dotted circles) can be tuned to facilitate different lasing chromaticities. Scale bar: 8 mm.

Conclusion

In conclusion, a facile strategy for the mass production of flexible multicolor lasing microfibers is demonstrated. The lasing properties can be tuned by regulating the doped dyes and solution viscosity. These lasing microfibers are further treated to be waterproof and are woven into textiles with a wide color gamut. Moreover, a woven lasing textile can be encrypted with a programmable lasing signal distribution by printing an NP pattern onto it to serve as an anticounterfeiting label for efficient authentication. This work unifies the fabrication and application of lasing textiles and may provide a pathway for manufacturing novel wearable lasing devices.
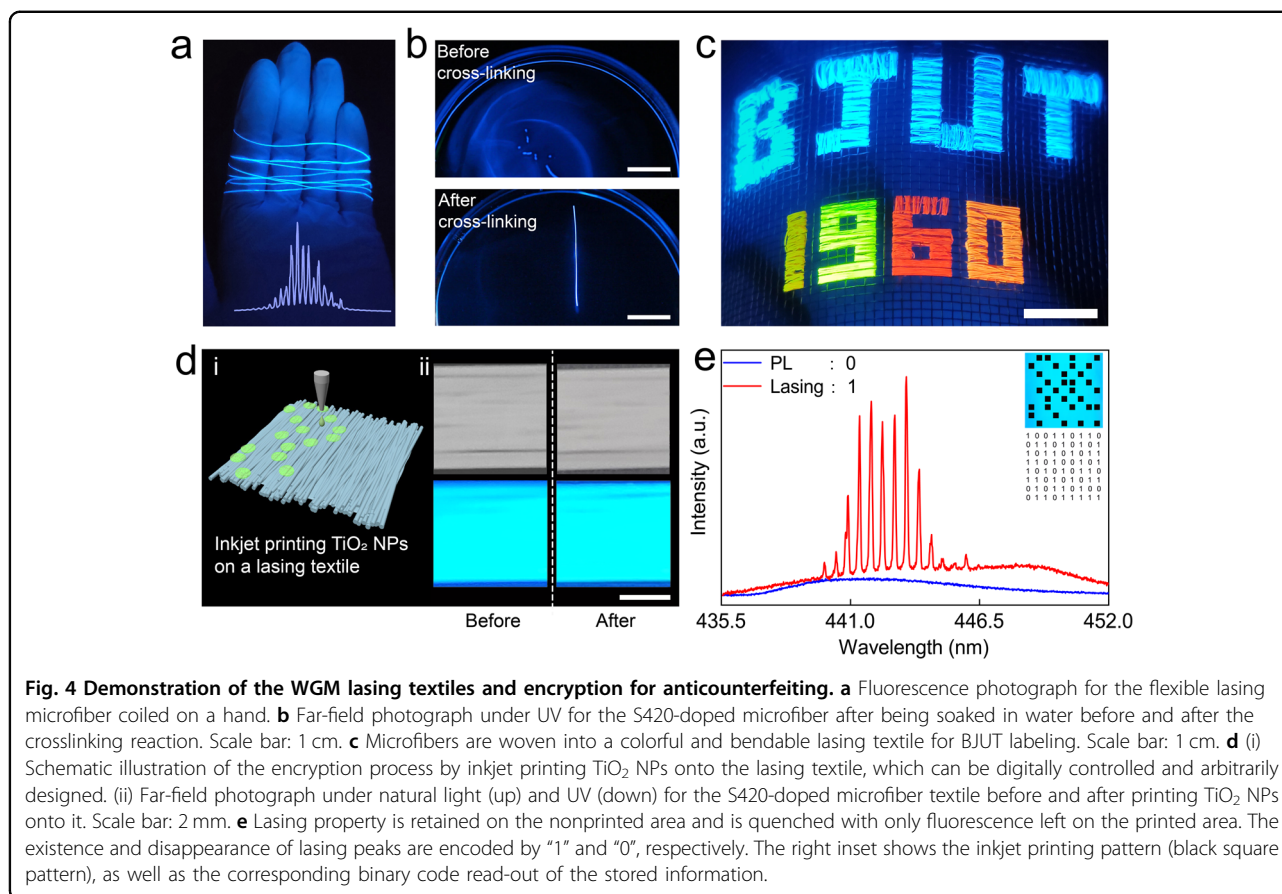
Materials and method
Preparation of microfibers

PVA (Mw: 198,000 g mol^{-1}) (1230 mg) was dissolved in deionized water (7 mL) at a concentration of approximately 176 mg mL^{-1}. Then, SDS and dyes were subsequently added to the solvated PVA. The concentration of SDS in the deionized water was regulated from 10 to 50 mg mL^{-1} (70–350 mg). The concentrations of the

emitting materials of S420, R6G, and RhB in deionized water were 12 mg mL^{-1} (84 mg), 3 mg mL^{-1} (21 mg), and 6 mg mL^{-1} (42 mg), respectively. For Uranin, 1 and 10 mg mL^{-1} (7 and 70 mg) were used to tune the emission, respectively. Finally, the mixed solutions were dispersed homogeneously by a magnetic stirrer at 60 °C for 6 h. The prepared solution was carefully loaded into a 2.5 mL syringe, and the squeezing flux was controlled by means of a microsyringe pump. In this experiment, the rotating speed of the drum was 3 rpm, and the squeezing flux of the solutions was controlled at 1 mL h^{-1}. For the mass production of the microfibers, the translational velocity of the syringe was 3 mm/s. The distance between the syringe tip and the drum collector was set at 17 cm for the formation of even filaments. The experiment was conducted in an ambient environment.

Lasing characterization

A nanosecond laser at a wavelength of 343 nm (third harmonics from a 1030 nm Yb:YAG laser, a repetition frequency of 200 Hz, and a pulse width of 1 ns) was coupled to a microscope connected to a PI spectrometer.

Fig. 4 Demonstration of the WGM lasing textiles and encryption for anticounterfeiting. a Fluorescence photograph for the flexible lasing microfiber coiled on a hand. **b** Far-field photograph under UV for the S420-doped microfiber after being soaked in water before and after the crosslinking reaction. Scale bar: 1 cm. **c** Microfibers are woven into a colorful and bendable lasing textile for BJUT labeling. Scale bar: 1 cm. **d** (i) Schematic illustration of the encryption process by inkjet printing TiO_2 NPs onto the lasing textile, which can be digitally controlled and arbitrarily designed. (ii) Far-field photograph under natural light (up) and UV (down) for the S420-doped microfiber textile before and after printing TiO_2 NPs onto it. Scale bar: 2 mm. **e** Lasing property is retained on the nonprinted area and is quenched with only fluorescence left on the printed area. The existence and disappearance of lasing peaks are encoded by "1" and "0", respectively. The right inset shows the inkjet printing pattern (black square pattern), as well as the corresponding binary code read-out of the stored information.

The emission spectra were collected by a spectrometer at 2400 g/mm.

Crosslinking of microfibers

A 5 M HCl solution was added to the mixed PVA-SDS dye solution to adjust its pH to 1. The acidified solution was used to prepare the microfibers. Then, the microfibers were treated with glutaraldehyde vapor in a sealed vessel for 24 h. After that, the as-crosslinked microfibers were submerged in deionized water to remove the excess glutaraldehyde and allowed to dry.

Inkjet printing

TiO_2 NPs (0.5 mg) were dispersed into 5 mL ethanol at a concentration of 0.1 mg mL^{-1}. The ink was printed on the lasing textile with a high-precision printer (Microfab JETLAB 4, Microfab Technologies Inc.) equipped with a 60-μm-diameter piezoelectric-driven inkjet nozzle. The experiment was conducted in an ambient environment.

Author contributions
J.R., D.G., and T.-R.Z. conceived the concept. J.R. and D.G. designed the experiments. J.R., B.N., and K.G. performed the experiments. J.R. and D.G. analyzed the data and wrote the manuscript. All authors discussed the results and commented on the manuscript.

Conflict of interest
The authors declare no competing interests.

References
1. Fan, W. et al. Iridescence-controlled and flexibly tunable retroreflective structural color film for smart displays. *Sci. Adv.* **5**, eaaw8755 (2019).
2. Wu, Y. Y., Mechael, S. S., Lerma, C., Carmichael, R. S. & Carmichael, T. B. Stretchable ultrasheer fabrics as semitransparent electrodes for wearable light-emitting e-textiles with changeable display patterns. *Matter* **2**, 882–895 (2020).
3. Hwang, Y. H. et al. Bright-multicolor, highly efficient, and addressable phosphorescent organic light-emitting fibers: toward wearable textile information displays. *Adv. Funct. Mater.* **31**, 2009336 (2021).

4. Shi, X. et al. Large-area display textiles integrated with functional systems. *Nature* **591**, 240–245 (2021).

5. Kwon, S. et al. Recent progress of fiber shaped lighting devices for smart display applications-a fibertronic perspective. *Adv. Mater.* **32**, 1903488 (2020).

6. Liang, J., Yan, Y. L. & Zhao, Y. S. Organic microlaser arrays: from materials engineering to optoelectronic applications. *Acc. Mater. Res.* **2**, 340–351 (2021).

7. Zhang, C. H. et al. Photonic skin based on flexible organic microlaser arrays. *Sci. Adv.* **7**, eabh3530 (2021).

8. Gu, Z. K. et al. Controllable growth of high-quality inorganic perovskite microplate arrays for functional optoelectronics. *Adv. Mater.* **32**, 1908006 (2020).

9. Wei, Q. et al. Recent progress in metal halide perovskite micro- and nanolasers. *Adv. Optical Mater.* **7**, 1900080 (2019).

10. Schlaus, A. P., Spencer, M. S. & Zhu, X. Y. Light-matter interaction and lasing in lead halide perovskites. *Acc. Chem. Res.* **52**, 2950–2959 (2019).

11. Zhang, Q., Shang, Q. Y., Su, R., Do, T. T. H. & Xiong, Q. H. Halide perovskite semiconductor lasers: materials, cavity design, and low threshold. *Nano Lett.* **21**, 1903–1914 (2021).

12. Huang, C. et al. Ultrafast control of vortex microlasers. *Science* **367**, 1018–1021 (2020).

13. He, L., Özdemir, Ş. K. & Yang, L. Whispering gallery microcavity lasers. *Laser Photonics Rev.* **7**, 60–82 (2013).

14. Yang, Y. D. et al. Whispering-gallery mode hexagonal micro-/nanocavity lasers. *Photonics Res.* **7**, 594–607 (2019).

15. Fan, Y. Q. et al. A universal in situ cross-linking strategy enables orthogonal processing of full-color organic microlaser arrays. *Adv. Funct. Mater.* **31**, 2103031 (2021).

16. Gu, F. X. et al. Single whispering-gallery mode lasing in polymer bottle microresonators via spatial pump engineering. *Light.: Sci. Appl.* **6**, e17061 (2017).

17. Zhou, Z. H. et al. Organic printed core–shell heterostructure arrays: a universal approach to all-color laser display panels. *Angew. Chem. Int. Ed.* **132**, 11912–11916 (2020).

18. Xu, Z. Y. et al. Multifunctional sensing based on an ultrathin transferrable microring laser. *ACS Appl. Mater. Interfaces* **13**, 19324–19331 (2021).

19. Krämmer, S. et al. Electrospun polymer fiber lasers for applications in vapor sensing. *Adv. Optical Mater.* **5**, 1700248 (2017).

20. Cheeney, J. E., Hsieh, S. T., Myung, N. V. & Haberer, E. D. Whispering gallery mode emission from dye-doped polymer fiber cross-sections fabricated by near-field electrospinning. *Nanoscale* **12**, 9873–9883 (2020).

21. Wang, C. L. et al. Programmable rainbow-colored optofluidic fiber laser encoded with topologically structured chiral droplets. *ACS Nano* **15**, 11126–11136 (2021).

22. Tang, S. J. et al. Laser particles with omnidirectional emission for cell tracking. *Light.: Sci. Appl.* **10**, 23 (2021).

23. Zhi, Y. Y., Yu, X. C., Gong, Q. H., Yang, L. & Xiao, Y. F. Single nanoparticle detection using optical microcavities. *Adv. Mater.* **29**, 1604920 (2017).

24. He, L., Ozdemir, S. K., Zhu, J. G., Kim, W. & Yang, L. Detecting single viruses and nanoparticles using whispering gallery microlasers. *Nat. Nanotechnol.* **6**, 428–432 (2011).

25. Wang, Y. Y., Zeng, S. W., Humbert, G. & Ho, H. P. Microfluidic whispering gallery mode optical sensors for biological applications. *Laser Photonics Rev.* **14**, 2000135 (2020).

26. Zhang, C. H. et al. Dual-color single-mode lasing in axially coupled organic nanowire resonators. *Sci. Adv.* **3**, e1700225 (2017).

27. Rueda, A., Sedlmeir, F., Kumari, M., Leuchs, G. & Schwefel, H. G. L. Resonant electro-optic frequency comb. *Nature* **568**, 378–381 (2019).

28. Fan, Y. Q. et al. Randomly induced phase transformation in silk protein-based microlaser arrays for anticounterfeiting. *Adv. Mater.* **33**, 2102586 (2021).

29. Shi, X. Y., Song, W. T., Guo, D., Tong, J. H. & Zhai, T. R. Selectively visualizing the hidden modes in random lasers for secure communication. *Laser Photonics Rev.* **15**, 2100295 (2021).

30. Zhu, S. et al. Flexible manipulation of lasing modes in an erbium-doped microcavity via an add–drop configuration. *ACS Photonics* **8**, 3069–3077 (2021).

31. Liang, W. et al. High spectral purity Kerr frequency comb radio frequency photonic oscillator. *Nat. Commun.* **6**, 7957 (2015).

32. Sebastian, S., Kailasnath, M., Nampoori, V. P. N. & Asokan, S. Ag nanowire-assisted low threshold WGM lasing from polymer optical fiber. *Opt. Lett.* **42**, 3820–3823 (2017).

33. Ta, V. D., Chen, R., Ma, L., Ying, Y. J. & Sun, H. D. Whispering gallery mode microlasers and refractive index sensing based on single polymer fiber. *Laser Photonics Rev.* **7**, 133–139 (2013).

34. Ta, V. D., Chen, R. & Sun, H. D. Controllable polarization of lasing emission from a polymer microfiber laser. *Sci. Rep.* **9**, 17017 (2019).

35. Sun, H., Zhang, Y., Zhang, J., Sun, X. M. & Peng, H. S. Energy harvesting and storage in 1D devices. *Nat. Rev. Mater.* **2**, 17023 (2017).

36. de Oliveira, M. C. A. et al. Dye-doped electrospun fibers for use as random laser generator: The influence of spot size and scatter concentration. *Opt. Mater.* **101**, 109722 (2020).

37. Henderson, D., Segur, H., Smolka, L. B. & Wadati, M. The motion of a falling liquid filament. *Phys. Fluids* **12**, 550–565 (2000).

38. Ravichandran, S. & Thaya Kumari, C. R. Effect of anionic surfactant on the thermo acoustical properties of sodium dodecyl sulphate in polyvinyl alcohol solution by ultrasonic method. *E-J. Chem.* **8**, 77–84 (2011).

39. Conto, F. P., Marin, J. F., Antkowiak, A., Castrejon-Pita, J. R. & Gordillo, L. Shape of a recoiling liquid filament. *Sci. Rep.* **9**, 15488 (2019).

40. Luo, M. R. The quality of light sources. *Color. Technol.* **127**, 75–87 (2011).

41. Luo, Z. Y., Chen, Y. & Wu, S. T. Wide color gamut LCD with a quantum dot backlight. *Opt. Express* **21**, 26269–26284 (2013).

42. Yang, Y. S. et al. Multicolor graphene quantum dots via solvatochromic tuning and sulfur doping for light-emitting diodes. *ACS Appl. Nano Mater.* **4**, 12325–12334 (2021).

43. Destaye, A. G., Lin, C. K. & Lee, C. K. Glutaraldehyde vapor cross-linked nano-fibrous PVA mat with in situ formed silver nanoparticles. *ACS Appl. Mater. Interfaces* **5**, 4745–4752 (2013).